Vol 460|13 August 2009|doi:10.1038/nature08263

LETTERS

Glacial effects limiting mountain height

D. L. Egholm[1], S. B. Nielsen[1], V. K. Pedersen[1] & J.-E. Lesemann[1]

The height of mountain ranges reflects the balance between tectonic rock uplift, crustal strength and surface denudation. Tectonic deformation and surface denudation are interdependent, however, and feedback mechanisms—in particular, the potential link to climate—are subjects of intense debate[1,2]. Spatial variations in fluvial denudation rate caused by precipitation gradients are known to provide first-order controls on mountain range width, crustal deformation rates and rock uplift[3,4]. Moreover, limits to crustal strength[5] are thought to constrain the maximum elevation of large continental plateaus, such as those in Tibet and the central Andes. There are indications that the general height of mountain ranges is also directly influenced by the extent of glaciation through an efficient denudation mechanism known as the glacial buzzsaw[6–9]. Here we use a global analysis of topography and show that variations in maximum mountain height correlate closely with climate-controlled gradients in snowline altitude for many high mountain ranges across orogenic ages and tectonic styles. With the aid of a numerical model, we further demonstrate how a combination of erosional destruction of topography above the snowline by glacier-sliding and commensurate isostatic landscape uplift caused by erosional unloading can explain observations of maximum mountain height by driving elevations towards an altitude window just below the snowline. The model thereby self-consistently produces the hypsometric signature of the glacial buzzsaw, and suggests that differences in the height of mountain ranges mainly reflect variations in local climate rather than tectonic forces.

Distinctive alpine landforms, such as broad 'U'-shaped, flat-floored valleys, hanging valleys, cirques, horns and knife-edged ridges (arêtes), are considered the fingerprints of glacial erosion. These glacial landforms exist in most of Earth's mountain chains, produced by present and past glaciers. A majority of these landforms are associated with pronounced topographic relief consisting of over-steepened valley sides, headwalls and near-orthogonal tributary junctions often occupied by spectacular waterfalls. Perhaps not surprisingly, glaciations have accordingly been assumed to increase average relief mainly by incising valley systems, leaving high elevation peaks and hillslopes almost unaffected, and producing significant isostatically driven peak uplift[10].

However, it has recently been discovered that glaciated orogens in the Himalayas[6], the Andes[7], the Sierra Nevada (USA)[11] and the Cascade Range[8] hold a striking coincidence of snowline altitudes, glacier equilibrium line altitudes (ELA) and elevations with a high proportion of surface area, suggesting that operation of a glacial buzzsaw denudation mechanism may be effective in reducing surface topography above the snowline and concentrating it at the snowline.

Apatite ^{4}He/^{3}He ratio and (U–Th)/He thermochronometry studies from British Columbia[12] and the St Elias orogen in Alaska[13] support the notion of rapid glacial erosion at altitudes near and above the snowline, and indicate that climatically controlled snowline lowering dramatically increased average erosion rates during the late Cenozoic.

The geomorphic signature of the glacial buzzsaw is a concentration of surface area at elevations corresponding to the glacial ELA or the snowline[6–9,11], which roughly coincide for temperate glaciers[14]. In hypsometric distributions (Fig. 1a), this reveals itself as a local maximum (representing a high proportion of surface area) at an altitude corresponding to the snowline[6,15]. To explore the prevalence of the glacial buzzsaw, we thus analysed the global distribution of hypsometric maxima (Fig. 1b) and surface area (Fig. 1c) using the Shuttle Radar Topography Mission[16] (SRTM) digital elevation models (DEMs) and compared this with observations of modern and Last Glacial Maximum (LGM) snowline altitudes[17,18]. We focus on the latitude dependence because the variation in snowline altitude is larger with latitude than with longitude (or with time); see Supplementary Figs 1–4 for more details of the analysis.

The analysis first reveals how only little surface area and practically no hypsometric maxima occur at elevations above the local modern snowline altitude (Fig. 1b and c). Second, below the snowline, surface area is concentrated in readily recognizable tectonically uplifted plateaus and near sea level, where alluvial plains increasingly dominate as they grade to sea level (Fig. 1c). The modern snowline seems to closely follow the 10^{-6} contour of normalized surface area (the blue end of the colour scale in Fig. 1c), emphasizing its influence on high-altitude hypsometry.

When a DEM tile has topography above the snowline, its highest hypsometric maximum generally exists between the modern and LGM snowlines (Fig. 2). This pattern is recognized globally in every mountain range with sufficient height to intersect the LGM snowline (Supplementary Fig. 4). Hence, the abundance of hypsometric maxima just below the modern snowline and the absence of hypsometric maxima above the snowline are largely independent of tectonic uplift rate, lithology and general tectonic setting. For example, the Himalayas are in an intra-continental setting caused by continent–continent collision between India and Asia, whereas the high topography in western North and South America and in New Zealand is adjacent to oceans and caused by subduction and related volcanism. Yet, all show similar correlation between the distribution of hypsometric maxima and the local snowline altitude.

It further appears that glacial erosion controls the maximum height of mountains, as most summit elevations are confined to altitudes $<$1,500 m above the local snowline (Fig. 2). Although some of the highest peaks are evidently not included in the analysis owing to data gaps, this general trend suggests that glacial erosion restricts the height of mountains by limiting the relief that can be maintained between mountain peaks and the snowline[1]. The recorded outliers (Fig. 2) represent solitary peaks of primarily volcanic origin and most exist in the Andes, implying that formation and ongoing build-up of high volcanoes can outpace glacial buzzsaw denudation. Notable exceptions to the trend also exist in the Transantarctic Mountains outside the data set where a reduction or even non-existence of the glacial buzzsaw mechanism is likely, as non-eroding polar glaciers (frozen at the bed) dominate where the ice cover is relatively thin[19].

[1]Department of Earth Sciences, Aarhus University, DK-8000 Aarhus, Denmark.

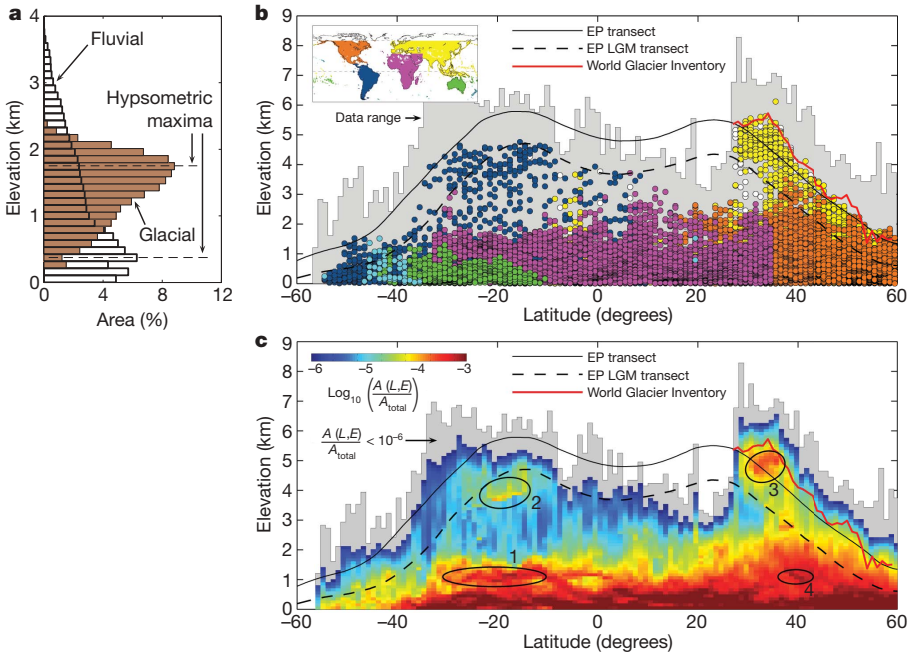

Figure 1 | Global prevalence of the glacial buzzsaw. **a**, Hypsometric distributions from a fluvial (northern Andes) and a glacial (Cascade Range, USA) landscape. Both hypsometries contain local maxima, but at different elevations. The hypsometric distributions each represent a $1^\circ \times 1^\circ$ DEM with coordinates (lower left corner) (09° N, 71° W) for the fluvial landscape and (48° N, 121° W) for the glacial. **b**, Global distribution of hypsometric maxima as function of latitude and elevation. Each hypsometric maximum found in the data set is represented by a circle coloured by its DEM database entry (upper left inset). Hypsometric maxima derived from DEMs with more than 5% data gaps are white. The grey shaded area represents the total data coverage set by the maximum elevation at each latitude. Also shown are the modern (black line) and LGM (dashed line) snowline transects along the east Pacific (EP) coasts of North and South America[17] and more than 13,000 modern snowline observations from the World Glacier Inventory[18] averaged in bins of 1° latitude where available (red line). **c**, Distribution of surface area (A) based on latitude (L) and elevation (E) within the data set. Colours show area at a given latitude and elevation normalized by the total area (A_{total}) of the data set. Note the logarithmic colour scale. The grey zone has very little area and falls outside the colour scale, but serves to outline the total data range. Ellipses mark tectonically uplifted plateaus: 1, South Africa; 2, the Altiplano (Andes), 3, the Tibetan plateau; and 4, the Tarim basin. (See also Supplementary Figs 1–4.)

Generally, the presence of a hypsometric maximum indicates that dynamic processes (tectonic, erosional or depositional) concentrate surface elevation within a narrow altitude interval. Thus, the high density of hypsometric maxima at low elevation (Fig. 1b and Supplementary Fig. 2) reflects, among other processes, fluvial erosion and deposition controlled by a base level ultimately set by the sea. Following this reasoning, and the findings of others[6–9,11,15], the abundance of hypsometric maxima associated with snowline altitudes and the general absence of hypsometric maxima above the snowline (Fig. 1) likewise suggest that glaciers concentrate surface area just below the snowline, which thereby acts like a local base level for glacial erosion, leaving only a limited amount of topography (horns and arêtes) rising above this level[6] (Fig. 1c). In large trunk valleys and fjords, glacial erosion is, however, known to reach far below the snowline[20].

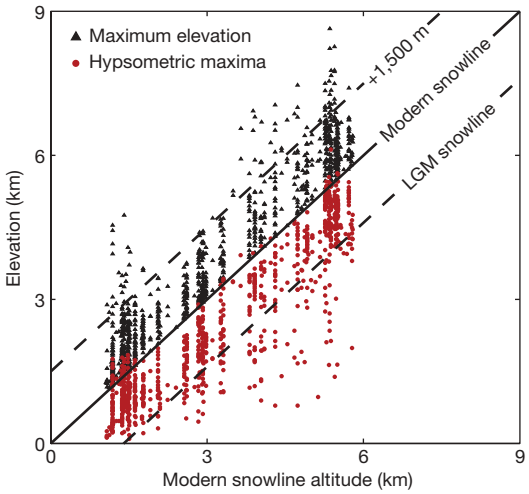

Figure 2 | Maximum elevations and hypsometric maxima elevations correlate with local snowline altitudes. Shown are all maximum DEM elevations (peaks) above the modern snowline and their associated highest hypsometric maxima. Most peaks are less than 1,500 m above the snowline, and apart from few exceptions all hypsometric maxima are found below the modern snowline and less consistently above the LGM snowline (the two snowlines largely demarcate the amplitude of the late Cenozoic climate variations). At latitudes >27° N, local snowline observations[18] (latitude- and longitude-dependent) are used, whereas the east Pacific snowline transects[17] are used independent of longitude for DEMs with latitude <27° N.

This erosional pattern is confirmed by computational model experiments coupling the flow equations of ice with glacial erosion driven by sliding of warm-based glaciers. As an example illustrating the imprint of glacial erosion, we simulate the evolution of an initially fluvial landscape during a dramatic lowering of the snowline altitude. The Sierra Nevada mountain range in southern Spain (37° N, 3° W) is used as the initial landscape as it was little affected by Quaternary glaciations, and only few cirque valleys near the highest summit areas above 2,500 m bear testimony to the past appearance of alpine glaciers. The landscape is thus largely fluvial (Fig. 3a), with relatively narrow river valleys emanating from the 60-km-long central ridge running broadly east–west. Accordingly, the hypsometric distribution derived from SRTM data[16] shows gradual decrease of surface area with increasing height above the 1,300 m contour line and with no indication of a local maximum (Fig. 3b).

To fully isolate the effects of glacial erosion and isostasy, the model does not include tectonic uplift, fluvial erosion or periglacial processes. In order to prevent slopes from steepening unrealistically, the model does, however, include nonlinear hillslope diffusion simulating mass wasting on the steepest slopes[21]. In the model, the snowline

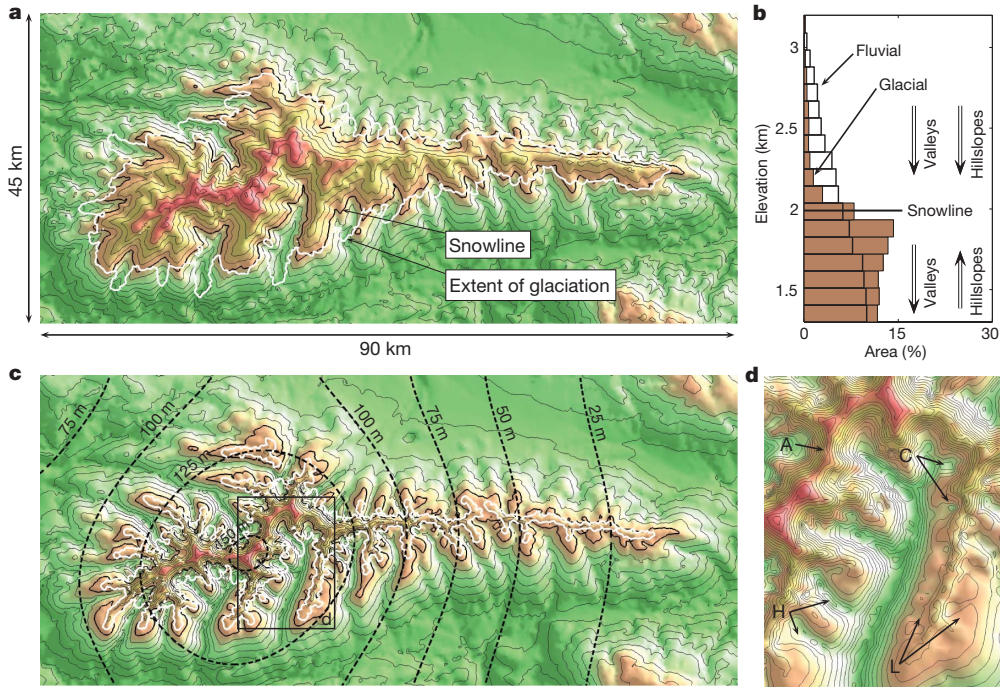

Figure 3 | Numerical model of glacial erosion in the Sierra Nevada (Spain). **a**, Initial fluvial topography derived from 90 m SRTM data[16]. The thick black contour line represents the model snowline altitude after 100 kyr, while the white contour line shows the extent of glaciers at time 100 kyr. **b**, Hypsometry before and after glacial erosion. A hypsometric maximum develops owing to denudation of hillslopes and small valleys above the snowline combined with isostatic uplift of unglaciated surfaces below the snowline. To some degree, the deep erosion of trunk valleys opposes the development of a hypsometric maximum by lowering their surface area to elevations far below the snowline. **c**, Model topography after glacial erosion to a stage where only narrow and steep ridges (arêtes) remain above the snowline. Valleys are widened and deepened below the snowline. The amplitudes of isostatic rock uplift are shown by dashed contour lines. **d**, Enlarged view of a catchment exhibiting classical glacial erosion features including arêtes (A), cirques (C), hanging valleys (H), and low relief areas (L) produced by the glacial buzzsaw. For more information on model results, see Supplementary Figs 5–10.

altitude is reduced from 3,000 m to 2,000 m (comparable to a 20° northward shift and conditions as found at present in, for example, British Columbia, Canada) over a period of 100 kyr, and in this stage the total ice volume grows until a quasi-steady state balance between total glacier accumulation and ablation is established. This leads into a longer phase (400 kyr) of glacial erosion and isostatic compensation. Although isostasy causes peak uplift[22], the ice volume decreases owing to overall erosional destruction of catchment area above the snowline. Hence, after 500 kyr the total ice volume is reduced to 20% of its maximum value (Supplementary Fig. 5).

In agreement with the glacial buzzsaw hypothesis, this model experiment reveals (Fig. 3b) how snowline lowering self-consistently leads to emergence of a hypsometric maximum just below the snowline owing to erosion of surface topography at, and above, the snowline and compensatory isostatic uplift affecting the entire landscape, including unglaciated hillslopes at lower altitudes.

The model results also highlight the variable influence of topography on ice flow. Trunk valley glaciers initially reach far below the snowline and cause deep valley incision. Their large catchments allow for sufficient ice flux below the snowline and erosion along most portions of the glacier in this region. The largest tributary catchments undergo more limited erosion than trunk valleys and develop hanging valleys, which often exhibit cirques near their headwalls (Fig. 3c and d). In smaller tributaries and on hillslopes, the key control on erosion appears to be the limited catchment area, which does not allow for ice influx to exceed ablation below the snowline and, in effect, the snowline acts like a climatic base level limiting the downvalley extent of glacial erosion. Glaciers with small catchment areas are thus fundamentally restricted by the snowline and unable to incise the landscape much below this level. Instead, they slowly erode headward into the landscape, leaving behind low-relief surfaces (Fig. 3d) at an altitude just below the snowline: the signature of the glacial buzzsaw. These low-relief surfaces are, however, separated by pronounced overdeepening in trunk valleys.

Isostatic uplift varies from ~200 m in the centre of the mountain range to 20 m in the upper right corner of the model (Fig. 3c). Thus, surface elevation increases in areas of the model where erosion rates are low. This applies to the highest arêtes and peaks as well as the lower parts of the hillslopes, which before glacial erosion were at altitudes below the snowline and therefore unglaciated. When the latter undergo isostatic uplift, some eventually pass the snowline and experience modification by glacial erosion as described above and further add to the hypsometric maxima.

In addition to classical features of alpine glaciation ('U'-shaped valleys, hanging valleys, overdeepenings, ridges and cirques; Fig. 3d), our model thus predicts that alpine glacial landscapes will naturally undergo strong erosion at and above the snowline. This erosion and its coupling with flexural isostasy produce the high proportion of surface area below the snowline, in agreement with global hypsometric observations. The concentration of surface area occurs in the temperature window (~0 °C) where periglacial processes (not included in the present model) are most effective. Thus, low-relief landscapes in the vicinity of the snowline will probably be further developed by frost cracking and frost creep[23]. This will effectively plane off and further flatten remnant short-wavelength topography into smooth low-curvature surfaces similar to those documented in the Laramide ranges of the western United States[23–25].

Active tectonic uplift counteracts the erosional destruction of topography above the snowline or balances it[26], but the evidence presented here and the results of other studies[6–9,11–13] indicate that glacial buzzsaw erosion is capable of keeping pace with any modern tectonic uplift rate. Therefore, the relationship between tectonism and climate is such that climate and latitude ultimately control the height to which tectonic processes can drive topography[6,7].

METHODS SUMMARY

The SRTM data set covers all land area within 120° of latitude (60° S to 60° N). Each of the 14,546 DEMs samples an area of $1^\circ \times 1^\circ$ with 3-arcsec resolution. For every DEM, we calculated the hypsometric distribution using 40 bins uniformly spaced between the DEM's minimum and maximum values, and systematically sampled the elevation(s) to any existing local maximum (see Supplementary Figs 1–4 for more details on the topographic analysis).

In the numerical model, the general treatment of ice motion and glacial erosion closely resembles other two- and three-dimensional models[27–29] of glacial landscape evolution. The numerical model is however based on the second-order shallow ice approximation[30] (SOSIA), which allows for simulating long-term glacier evolution at a higher resolution by accounting for important higher-order effects related to a rugged basal topography, rapid ice flow accelerations, and large gradients in longitudinal stress and ice thickness.

Full Methods and any associated references are available in the online version of the paper at www.nature.com/nature.

Received 27 February; accepted 29 June 2009.

1. Whipple, K. X., Kirby, E. & Brocklehurst, S. H. Geomorphic limits to climate-induced increases in topographic relief. *Nature* **401,** 39–43 (1999).
2. Whipple, K. X. The influence of climate on the tectonic evolution of mountain belts. *Nature Geosci.* **2,** 97–104 (2009).
3. Beaumont, C., Fullsack, P. & Hamilton, J. in *Thrust Tectonics* (ed. McClay, K. R.) 1–18 (Chapman & Hall, 1992).
4. Willett, S. D. Orogeny and orography: the effects of erosion on the structure of mountain belts. *J. Geophys. Res.* **104,** 28957–28981 (1999).
5. Beaumont, C., Jamieson, R. A., Nguyen, M. H. & Medvedev, S. Crustal channel flows: 1. Numerical models with application to the tectonics of the Himalayan-Tibetan orogen. *J. Geophys. Res.* **109,** B06406 (2004).
6. Brozovic, N., Burbank, D. & Meigs, A. Climatic limits on landscape development in the northwestern Himalaya. *Science* **276,** 571–574 (1997).
7. Montgomery, D. R., Balco, G. & Willett, S. D. Climate, tectonics, and the morphology of the Andes. *Geology* **29,** 579–582 (2001).
8. Mitchell, S. G. & Montgomery, D. R. Influence of a glacial buzzsaw on the height and morphology of the Cascade Range in central Washington State, USA. *Quat. Res.* **65,** 96–107 (2006).
9. Foster, D., Brocklehurst, S. H. & Gawthorpe, R. L. Small valley glaciers and the effectiveness of the glacial buzzsaw in the northern Basin and Range, USA. *Geomorphology* **102,** 624–639 (2008).
10. Molnar, P. & England, P. Late Cenozoic uplift of mountain ranges and global climate change: chicken or egg? *Nature* **346,** 29–34 (1990).
11. Brocklehurst, S. H. & Whipple, K. X. Glacial erosion and relief production in the Eastern Sierra Nevada, California. *Geomorphology* **42,** 1–24 (2002).
12. Shuster, D. L., Ehlers, T. A., Rusmoren, M. E. & Farley, K. A. Rapid glacial erosion at 1.8 Ma revealed by ^{4}He/^{3}He thermochronometry. *Science* **310,** 1668–1670 (2005).
13. Berger, A. L. & Spotila, J. A. Denudation and deformation in a glaciated orogenic wedge: the St. Elias orogen, Alaska. *Geology* **36,** 523–526 (2008).
14. Paterson, W. S. B. *The Physics of Glaciers* 3rd edn (Butterworth-Heinemann, 1994).
15. Brocklehurst, S. H. & Whipple, K. X. Hypsometry of glaciated landscapes. *Earth Surf. Process. Landforms* **29,** 907–926 (2004).
16. Farr, T. G. *et al.* The Shuttle Radar Topography Mission. *Rev. Geophys.* **45,** RG2004, doi:10.1029/2005RG000183 (2007).
17. Broecker, W. S. & Denton, G. H. The role of ocean-atmosphere reorganizations in glacial cycles. *Geochim. Cosmochim. Acta* **53,** 2465–2501 (1989).
18. National Snow and Ice Data Center. World glacier inventory (2009). ⟨http://nsidc.org/data/docs/noaa/g01130_glacier_inventory⟩.
19. Stern, T. A., Baxter, A. K. & Barrett, P. J. Isostatic rebound due to glacial erosion within the Transantarctic Mountains. *Geology* **33,** 221–224 (2005).
20. Brocklehurst, S. H. & Whipple, K. X. Assessing the relative efficiency of fluvial and glacial erosion through simulation of fluvial landscapes. *Geomorphology* **75,** 283–299 (2006).
21. Roering, J. J., Kirchner, J. W. & Dietrich, W. E. Evidence for nonlinear, diffusive sediment transport and implications for landscape morphology. *Wat. Resour. Res.* **35,** 853–870 (1999).
22. Montgomery, D. R. Valley incision and the uplift of mountain peaks. *J. Geophys. Res.* **99,** 13913–13921 (1994).
23. Anderson, R. S. Modeling of tor-dotted crests, bedrock edges and parabolic profiles of the high alpine surfaces of the Wind River Range, Wyoming. *Geomorphology* **46,** 35–58 (2002).
24. Small, E. E. & Anderson, R. S. Pleistocene relief production in Laramide Mountain Ranges, western U.S. *Geology* **26,** 123–126 (1998).
25. Munroe, J. S. Investigating the spatial distribution of summit flats in the Uinta Mountains of northeastern Utah, USA. *Geomorphology* **75,** 437–449 (2006).
26. Brocklehurst, S. H. & Whipple, K. X. Response of glacial landscapes to spatial variations in rock uplift rate. *J. Geophys. Res.* **112,** F02035, doi:10.1029/2006JF000667 (2007).
27. Harbor, J. M., Hallet, B. & Raymond, C. F. A numerical model of landform development by glacial erosion. *Nature* **333,** 347–349 (1988).
28. MacGregor, K. R., Anderson, R. S., Anderson, S. P. & Waddington, E. D. Numerical simulations of glacial-valley longitudinal profile evolution. *Geology* **28,** 1031–1034 (2000).
29. Tomkin, J. H. & Braun, J. The influence of alpine glaciation on the relief of tectonically active mountain belts. *Am. J. Sci.* **302,** 169–190 (2002).
30. Baral, D. R., Hutter, K. & Greve, R. Asymptotic theories of large-scale motion, temperature, and moisture distribution in land-based polythermal ice sheets: A critical review and new developments. *Appl. Mech. Rev.* **54,** 215–256 (2001).

Supplementary Information is linked to the online version of the paper at www.nature.com/nature.

Acknowledgements We thank K. Hutter and N. Kirchner for assistance with the implementation of the SOSIA. We also thank C. Clark, J. A. Piotrowski, B. H. Jacobsen, M. Sandiford, R. Brown and O. Humlum for comments. J. Braun and S. Brocklehurst are thanked for reviews that improved the manuscript considerably.

Author Contributions D.L.E. and S.B.N. designed the study. V.K.P. and D.L.E. performed the global topographic analysis. D.L.E. implemented the SOSIA and performed the numerical modelling. All four authors contributed to writing the paper in the order listed.

Author Information Reprints and permissions information is available at www.nature.com/reprints. Correspondence and requests for materials should be addressed to D.L.E. (david@geo.au.dk).

METHODS

Overview. The present numerical landscape evolution model serves to demonstrate how the glacial buzzsaw denudation mechanism inherently follows from already established assumptions on glacier dynamics and glacial erosion. Compared to existing modelling studies[31–35], there are no new assumptions. The governing equations are, however, solved using a novel approach (Supplementary Information). This allows prediction of three-dimensional patterns of glacial erosion on a much finer scale than previously because it considers the effects of steep bed topography and gradients in horizontal stress within the ice. Importantly, this permits modelled erosion patterns to be analysed at the scale of the well-known glacial landforms (hanging valleys, cirque valleys, and so on).

The mechanism of glacial buzzsaw erosion is very robust when varying model parameters controlling, for example, ice flow velocities, erosion rates and subglacial water pressure. This is because the buzzsaw signal arises primarily because of ablation patterns caused by the atmospheric temperature gradient. In other words, the downward restriction of small glaciers does not depend on the exact nature of the ice flow, but on the fact that small glaciers quickly melt when passing the snowline altitude.

Modelling ice flow and glacial erosion. Ice motion is the sum of internal deformation and basal sliding. The internal deformation is governed by Glen's flow law, $\varepsilon_{ij} = A\tau_e{}^2\tau_{ij}$, relating components of the strain rate tensor, ε_{ij}, to components of the deviatoric stress tensor, τ_{ij}. τ_e is the effective stress[36] and $A = 2.25 \times 10^{-17}\,\mathrm{Pa}^{-3}\,\mathrm{yr}^{-1}$ is the Arrhenius constant for ice at temperatures around $-10\,^{\circ}\mathrm{C}$ (ref. 37).

The sliding velocity is assumed aligned with the basal shear stress, τ_s, and of magnitude given by the generalized Weertman law[38]: $u_s = C_s|\tau_s|^m/(p_i - p_w)^n$. Here $C_s = 2 \times 10^{-9}\,\mathrm{m\,Pa}^{-2}\,\mathrm{yr}^{-1}$ is a sliding coefficient, p_i is the ice overburden pressure normal to the bed and p_w is the meltwater pressure at the bed. We follow others[31–35] and assume a constant ratio between melt water and overburden pressures, $p_w = 0.2p_i$, and that $m = 3$ and $n = 1$. Although there is some experimental support[39,40] for the latter choice, m and n are poorly constrained parameters. We have, therefore, explored the sensitivity of the modelling results to variations in m and n, and in agreement with ref. 41 we find that changing the parameters mainly affects the shape of valleys and not our conclusions regarding erosional patterns of the buzzsaw denudation mechanism.

Mass balance is calculated as the sum of accumulation, M_a, surface ablation, M_s, and basal melting, M_b, all in units of $\mathrm{m\,yr}^{-1}$; $M_a = -0.1\min(0, T_s)$, $M_s = -0.15\max(0, T_s)$ and $M_b = -0.05\max(T_m, T_b)$. Here T_s (in units of $^{\circ}\mathrm{C}$), given by $T_0 - 5h$, is the ice surface temperature at altitude h (in units of km); T_b is basal temperature as predicted from one-dimensional temperature profiles including conduction and vertical advection of heat[32]; $T_m = -0.00087H$ is the melting point of ice (H is ice thickness in units of m). T_0 is reduced from $15\,^{\circ}\mathrm{C}$ to $10\,^{\circ}\mathrm{C}$ during the initial 100 kyr. The downward migration of the snowline allows wet-based glacial erosion to affect, at varying degrees and different times, all altitudes in the landscape above the final snowline altitude. This ensures that the highest peaks and arêtes (which after 100 kyr are in a temperature window with non-eroding cold-based ice) have experienced glacial erosion and gives them a realistic glacial appearance. The slow downwards migration of the snowline can be understood as (1) a slow and long-term average temperature decline (averaging shorter term second order variations) or (2) tectonic uplift that transports topography slowly upwards through the snowline altitude.

We assume that the local glacial erosion rate normal to the bed is primarily governed by abrasion and quarrying, and hence[42,43], proportional to local sliding rates: $e = k_e|u_s|$. k_e is calibrated to 1×10^{-4} by requiring average erosion rates to be less than $1\,\mathrm{mm\,yr}^{-1}$, which is a conservative estimate[42]. Depending on the altitude and the thickness of the ice, the model glaciers above the snowline can be frozen to the bed. The basal sliding rate is then zero and ice transport is solely due to internal deformation.

The Stokes mechanical equilibrium equations are solved using the second-order shallow ice approximation[36] (SOSIA) and a finite volume formulation (see Supplementary Information for details) with an irregular grid and explicit time integration. The higher-order method allows for solving the ice flow equations accurately, also when basal topography is steep and when significant gradients in longitudinal and transverse stress are present. The irregular grid consists of 31,480 Voronoi cells with average spacing of 400 m.

Modelling hillslope processes. In order to prevent surface slopes from increasing unrealistically, we include mass wasting on steep slopes using a nonlinear diffusion model[44,45]. The model expresses the flux of material, $q = -\kappa s/[1 - (s/s_c)^2]$, as a function of surface slope, s. $\kappa = 1\,\mathrm{m}^2\,\mathrm{yr}^{-1}$ is the diffusivity of low gradient hillslopes, while $s_c = 1.0$ defines a critical slope near which the effective diffusivity increases towards infinity.

Modelling flexural isostasy. Flexural isostasy is incorporated by coupling the erosion model to a two-dimensional uniform thin elastic plate[45] with an elastic thickness of 10 km. The densities of the eroding crust and the asthenosphere are $2{,}800\,\mathrm{kg\,m}^{-3}$ and $3{,}300\,\mathrm{kg\,m}^{-3}$, respectively. Erosional unloading and the weight of the ice cause deflections of the plate, which are fed back into the model as vertical surface movements. The relatively small size of the Sierra Nevada mountain range combined with the elastic thickness of 10 km effectively limits the amplitudes of isostatic uplift following erosion. The model presented is thus conservative with respect to how isostasy contributes to the mechanism of the glacial buzzsaw.

31. Harbor, J. M., Hallet, B. & Raymond, C. F. A numerical model of landform development by glacial erosion. *Nature* **333,** 347–349 (1988).
32. Braun, J., Zwartz, D. & Tomkin, J. A new surface-processes model combining glacial and fluvial erosion. *Ann. Glaciol.* **28,** 282–290 (1999).
33. MacGregor, K. R., Anderson, R. S., Anderson, S. P. & Waddington, E. D. Numerical simulations of glacial-valley longitudinal profile evolution. *Geology* **28,** 1031–1034 (2000).
34. Jamieson, S. S. R., Hulton, N. R. J. & Hagdorn, M. Modelling landscape evolution under ice sheets. *Geomorphology* **97,** 91–108 (2008).
35. Tomkin, J. H. Numerically simulating alpine landscapes: the geomorphologic consequences of incorporating glacial erosion in surface process models. *Geomorphology* **103,** 180–188 (2009).
36. Baral, D. R., Hutter, K. & Greve, R. Asymptotic theories of large-scale motion, temperature, and moisture distribution in land-based polythermal ice sheets: a critical review and new developments. *Appl. Mech. Rev.* **54,** 215–256 (2001).
37. Hooke, R. L. Flow law for polycrystalline ice in glaciers: comparison of theoretical predictions, laboratory data, and field measurements. *Rev. Geophys. Space Phys.* **19,** 664–672 (1981).
38. Paterson, W. S. B. *The Physics of Glaciers* 3rd edn (Butterworth-Heinemann, 1994).
39. Budd, W. F., Keage, P. L. & Blundy, N. A. Empirical studies of ice sliding. *J. Glaciol.* **23,** 157–170 (1979).
40. Bindschadler, R. The importance of pressurized subglacial water in separation and sliding at the glacier bed. *J. Glaciol.* **29,** 3–19 (1983).
41. Harbor, J. M. Application of a general sliding law to simulating flow in a glacier cross-section. *J. Glaciol.* **38,** 182–190 (1992).
42. Hallet, B. Glacial quarrying: a simple theoretical model. *Ann. Glaciol.* **22,** 1–8 (1996).
43. Humphrey, N. F. & Raymond, C. F. Hydrology, erosion and sediment production in a surging glacier: Variegated Glacier, Alaska, 1982-83. *J. Glaciol.* **40,** 539–552 (1994).
44. Roering, J. J., Kirchner, J. W. & Dietrich, W. E. Evidence for nonlinear, diffusive sediment transport and implications for landscape morphology. *Wat. Resour. Res.* **35,** 853–870 (1999).
45. Pelletier, J. *Quantitative Modeling of Earth Surface Processes* (Cambridge Univ. Press, 2008).